Journal of Nanobiotechnology

RESEARCH Open Access

High-throughput screening-based design of multifunctional natural polyphenol nanovesicles to accelerate diabetic wound healing

Xiaoying Zhao[1,2,3†], Shenkai Su[1,2,3†], Chenyu Wu[1,2,3], Yuxin Deng[1,2,3], Yu Chen[1,2,3], Tanxin Yu[1,2,3], Chenchao Li[1,2,3], Yekai Zhang[1,2,3†], Xiangyang Wang[1,2,3*], Yifei Zhou[1,2,3*] and Xiaolei Zhang[1,2,3*]

Abstract

Oxidative stress is a major pathological factor that impedes the diabetic wound healing process. Procyanidins (PC) form nanoparticle-vesicles (PPNs) through hydrogen bonding and exhibit good drug delivery capability; however, their application in diabetic wounds is unsatisfactory. To meet the antioxidant needs for treating, high-throughput screening in the natural product library (NPL) under in vitro oxidative stress conditions was conducted to enhance the antioxidant activity of PPNs. HUVECs treated with tert-Butyl Hydroperoxide (TBHP) were established as screening model in vitro. Baicalein (BAI) was identified from over 600 products in the library as the most effective one to combat oxidative stress. Further study showed that PC and BAI may react in equal proportions to synthesize new vesicles, named BAI-PC Polyphenolic nanovesicles (BPPNs), which possess reactive oxygen species (ROS) responsive and antioxidant effects. Network pharmacology indicated that in diabetic wounds, the target genes of PC are mainly enriched in the vascular endothelial growth factor (VEGF)-related pathways, while BAI primarily regulates tyrosine phosphorylation. The complementarity between the two has been validated in both in vitro and in vivo experiments. In summary, the antioxidant drug BAI, identified through high-throughput screening of NPL, could optimize the biological function of PPNs; the newly-synthesized BPPNs may accelerate diabetic wound healing through dual mechanisms of promoting angiogenesis and combating oxidative stress.

Introduction

Diabetic wounds are prevalent chronic, unhealing wounds. Wound healing is one of the most intricate processes within the human body, and it is broadly categorized into four phases: hemostasis, inflammation, proliferation, and remodeling. It involves the orchestrated regulation of various cell types over time and space [1]. Reactive oxygen species (ROS), which encompasses superoxide anions ($O_2^{-}\bullet$), peroxides, hydroxyl radicals ($OH\bullet$), and singlet oxygen ($^1O_2$) [2], serve as pivotal regulatory factors in various stages of wound healing. However, an excessive abundance of ROS can lead to oxidative damage in wound-edge cells, hastening cellular senescence and apoptosis, thereby impeding the overall

†XY Zhao, SK Su and YK Zhang are co-autors.

*Correspondence:
Xiangyang Wang
xiangyangwang@wmu.edu.cn
Yifei Zhou
yifeizhou@wmu.edu.cn
Xiaolei Zhang
zhangxiaolei@wmu.edu.cn

Full list of author information is available at the end of the article

Graphical abstract

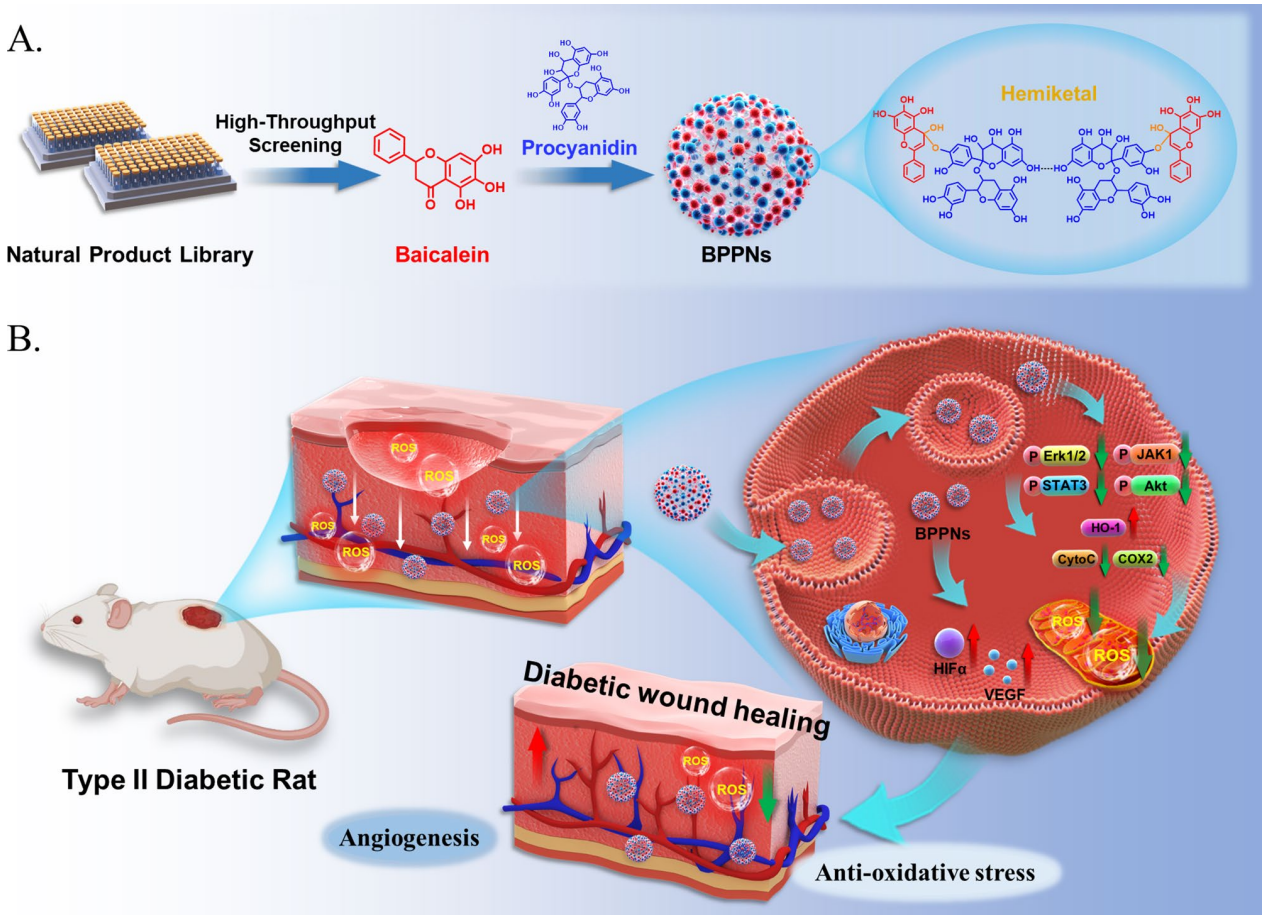

Keywords Natural product library, Polyphenol nanovesicles, Diabetic wound healing, Antioxidative stress, Peptidyl-tyrosine phosphorylation

wound healing process [3–5]. Research indicates that elevated blood glucose levels lead to an upregulation of pro-inflammatory factors, which in turn induces heightened oxidative stress [6]. Excessive oxidative stress in tissues and a diminished antioxidative capacity result in an oxidative-reductive imbalance, which stands as a primary determinant of the delayed wound healing process in diabetes [3, 7]. Therefore, anti-oxidative stress are important for treating diabetic wound healing .

General clinical treatment for wounds includes restoring skin perfusion, treating infections, controlling metabolism, managing comorbidities, and caring for local trauma. Although these standard treatments may achieve the goal of controlling symptoms, they still offer limited success in promoting wound healing in diabetes [8]. The demand for advanced biomaterials in wound healing is rapidly expanding. Biomaterials that allow for the controlled release of signaling molecules can be combined with other treatment methods, presenting a promising treatment method for diabetes wound healing [9, 10]. Nano-biomaterials have shown great potential in wound healing due to their multifunctionality and superior physicochemical properties.

Natural polyphenols are a class of compounds widely present in living organisms, known for their antioxidant, anti-inflammatory, anticancer, antibacterial, and antiviral effects, and are widely used in the treatment of various diseases [11]. In addition to having multiple biological functions, natural polyphenols also possess unique physicochemical properties, that allow them to form nanoparticles by combining with various substances such as drugs, proteins, nucleic acids, metal ions, etc. through hydrogen bonding, hydrophobic interactions, and electrostatic interactions [12, 13]. Studies have shown that natural polyphenols on the surface can effectively enhance the endocytosis of nanoparticles [14, 15].

Based on these characteristics, natural polyphenols are widely used in the manufacturing of biomaterials, such as nanoparticles [16], nanocapsules [17], encapsulation coatings [18], and so on.

Procyanidins (PC), a type of natural polyphenol, are considered a highly promising biomaterial with good bioactivity and biocompatibility [19, 20]. The structure of PC features a substantial presence of aromatic rings and phenolic hydroxyl groups confers both amphiphilic and amphiphobic characteristics. Furthermore, they readily engage in hydrogen bonding, governing non-covalent interactions and giving rise to intricate networks [12, 21]. Using these properties of the PC, a polyphenol bubble was synthesized, named "Procyanidins polyphenol nanovesicles (PPNs)". In pursuit of enhancing the antioxidative therapeutic potential of these polyphenol nanovesicles, we conducted a high-throughput drug screening utilizing the Natural Product Library (NPL), an assembly of natural compounds known for their exceptional safety profiles. From a selection of 622 natural compounds, we identified the most efficacious antioxidants and optimized the PPNs to achieve superior therapeutic outcomes in diabetic wound healing.

Results

Sustained high levels of oxidative stress in diabetic wound tissue

Existing research indicates that in normal wounds, oxidative stress primarily occurs within the initial three days following injury and gradually diminishes as the inflammatory phase subsides [7]. In contrast, diabetic wounds exhibit sustained, high levels of ROS [3]. To further substantiate the oxidative stress levels within diabetic wounds, we have established a rat model of diabetes mellitus (DM) following the protocol delineated in Fig. 1A. The monitoring of blood glucose in the Ctrl group and the DM group confirmed the successful establishment of the diabetes model (Fig. 1B). Subsequently, a full-thickness incision with a diameter of 20 mm was made on the dorsal surface of both the Ctrl group and the DM group rats. As illustrated in Fig. 1C, the postoperative wound healing process of both rat groups was documented at days 0, 1, 3, 5, 7, 14, and 21. Compared to Ctrl, the DM group exhibited a noticeably delayed wound healing process with a tendency towards non-closure (Fig. 1D). Considering the pivotal role of oxidative stress in wound healing, we examined the tissue oxidative stress levels at various stages of wound healing (Day 3 – the inflammatory phase, Day 7 – the proliferation phase, and Day 14 – the remodeling phase [1]) in both the Ctrl and DM

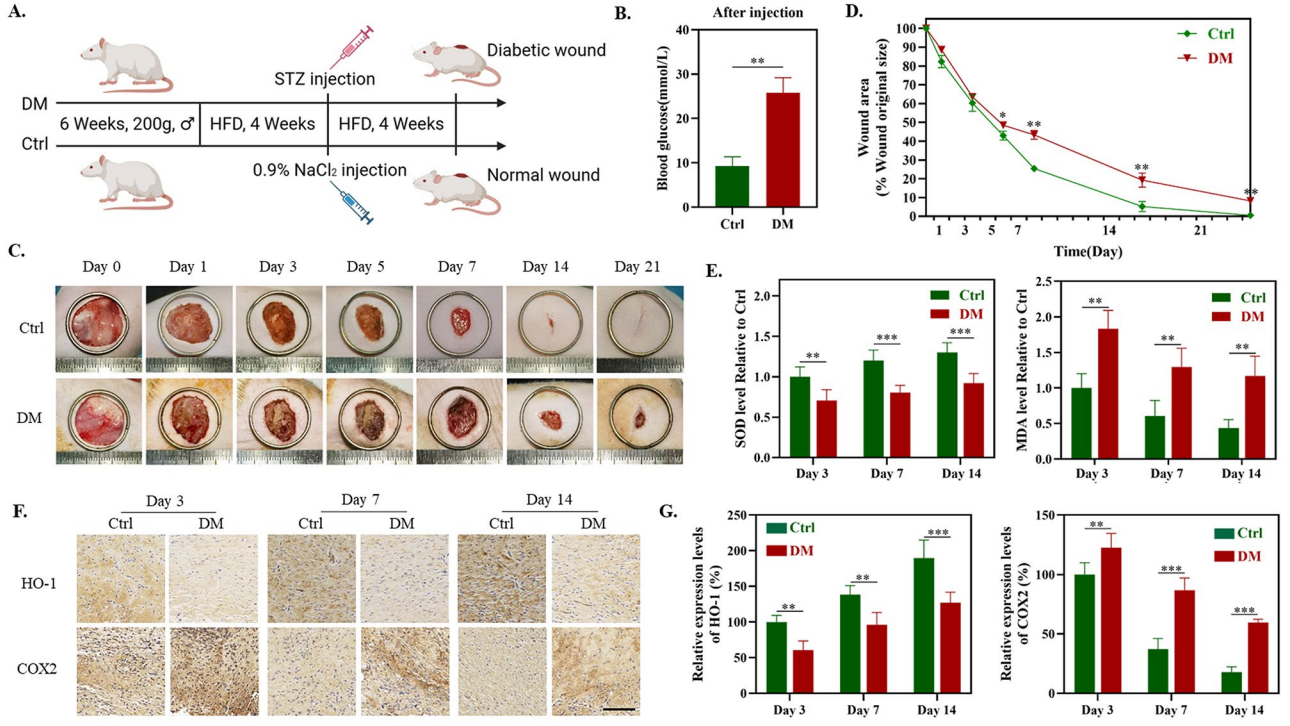

Fig. 1 Establishment of the Diabetic Wound Model and detection of oxidative stress levels in tissues. (**A**) Schematic representation of the establishment of the diabetic wound model. (**B**) Blood glucose levels in the control group (Ctrl) and the diabetic group (DM). (**C**) Representative photographs of diabetic wounds for Ctrl and DM groups on the 0, 1st, 3rd, 5th, 7th, 14th, and 21st day. (**D**) Quantitative analysis of wound area change in comparison with the original wound. (**E**) SOD and MDA level of Ctrl and DM on day 3, 7 and 14. (**F**) Corresponding immunohistochemistry staining of COX2 and HO-1 on day 3, 7 and 14. (**G**) Immunohistochemical quantification of COX2 and HO-1 in image F ($n = 5$). $^{*}P < 0.05$, $^{**}P < 0.01$, $^{***}P < 0.005$

groups. The results indicate that, whether on the 3rd, 7th, and 14th day of wound healing, the DM group exhibited significantly lower activities of superoxide dismutase (SOD) and protein expression of heme oxygenase-1 (HO-1) compared to the Ctrl group. Moreover, the levels of lipid peroxidation (malondialdehyde, MDA) and expression of cyclooxygenase-2 (COX2) were notably higher in the DM group than in the Ctrl group (Fig. 1E-G). The aforementioned experimental results indicate that, in comparison to normal wounds, diabetic wound tissues consistently maintain high levels of oxidative stress throughout the entire wound healing process, corroborating previous research findings.

High-throughput screening of natural product libraries and network pharmacology analysis

To better target oxidative stress and improve the therapeutic effect on diabetic wounds, this study used TBHP (100 μM) to induce oxidative stress in HUVECs in vitro, and a high-throughput screening was conducted on the natural product library (NPL) consisting of 622 compounds (Figure S1A). The specific procedure is illustrated in Fig. 2A, where cell viability is employed as an indicator of a drug's capacity for antioxidant stress. Toxicity tests were conducted on the top five ranking drugs based on cell viability to ascertain the optimal dosages for these five drugs (Figure S1B). At the optimal concentration, the fluorescence intensity of DCFH-DA was utilized to assess the ROS scavenging capabilities of these five compounds (Fig. 2B). Subsequently, baicalein (BAI, 5 μM), which exhibited the most remarkable antioxidative effect in HUVECs, was selected for further investigations.

Using network pharmacology, a Venn diagram was constructed to elucidate the predicted targets of PC and BAI, as well as the disease-related targets involved in diabetic wound healing. Additionally, common targets shared by these compounds were identified (Fig. 2C and S1C). In order to investigate the respective effects of biological materials and pharmaceuticals on disease treatment, we conducted separate Gene Ontology (GO) Enrichment Analysis for the common targets of BAI and PC that intersect with the disease but do not overlap. The results of the enrichment analysis indicate that BAI may influence on peptidyl-tyrosine phosphorylation and cellular response to hydrogen peroxide (Fig. 2D), whereas PC primarily affects the vascular endothelial growth factor receptor signaling pathway (Fig. 2E). This suggests that BAI and PC exhibit a potential complementarity in therapeutic efficacy, and their combined action may influence wound healing through distinct processes, namely antioxidant stress and angiogenesis. This opens up the possibility of multifunctional optimization for PPNs.

Synthesis and characterization of baicalein-procyanidins polyphenol nanovesicles (BPPNs)

PC can utilize the physical adsorption of $CaCO_3$ on polyphenols to form vesicles [22, 23], which can denucleate into PPNs under acidic conditions. Under the same conditions, new polyphenol vesicles, BPPNs were synthesized using equal amounts of PC and BAI. PPNs and BPPNs are collectively referred to as "Polyphenol nanovesicles (PNs)". As shown in Fig. 3A, the scanning electron microscopy (SEM) image of PPNs and BPPNs shows that BPPNs are spherical vesicles with a diameter smaller than PPNs. The diameter and Zeta potential of both were measured, and it was found that the diameter of BPPNs was about 500 nm, which is half of PPNs, and the Zeta potential of BPPNs was similar to PPNs, indicating that the addition of BAI reduced the size of the vesicles without affecting their stability (Fig. 3B). The FTIR spectra of BAI, PPNs, and BPPNs are depicted in Fig. 3C. No free hydroxyl peak can be found in PPNs, as indicated by a broad absorption peak at 3310 cm^{-1}, suggesting that hydroxyl hydrogen bonds bind PC molecules connected [12]. The BPPNs inherit the phenolic hydroxyl absorption peak exposed by BAI (3409 cm^{-1}), signifying that, at a chemical level, the newly synthesized nanoparticles exhibit enhanced antioxidative properties. Furthermore, in comparison to BAI, BPPNs exhibit no absorption peak around 1655 cm^{-1}, implying that the ketone carbonyl disappeared during the synthesis process of the nanovesicles, a possible addition reaction occurred between the carbonyl group in the BAI structure and the phenolic hydroxyl group in PC. This potentially led to the formation of hemiketals that effectively preserve the chemical structure of BAI. Besides, the addition of BAI results in a significant weakening of the infrared absorption peaks and the disappearance of certain group vibrations, as observed in the BPPNs' FTIR spectrum. This suggests that intermolecular forces are formed between BAI and PC. Given the presence of phenolic hydroxyl groups, we can infer that the intermolecular forces at least involve hydrogen bonding [12]. The presence of intermolecular forces also explains the reduction in particle size, which is attributed to heterogeneous nucleation [24]. Based on this, create a synthesized illustrative diagram as depicted in Fig. 3D. Analyzing from a chemical perspective, the hemiketals can protect the carbonyl structure in BAI, decompose after pH change, and release complete BAI and PC molecules under the mildly acidic environment found in diabetic wounds [25], respectively playing their respective therapeutic roles. According to the molecular formula (PC: $C_{30}H_{26}O_{13}$, BAI: $C_{15}H_{10}O_5$) and XPS analysis of PNs involving carbon (C) and oxygen (O) atoms, the results indicate that the content of PC and BAI in BPPNs is approximately in a 1:1 ratio (Fig. 3E). The peak fitting results also confirmed the successful synthesis of

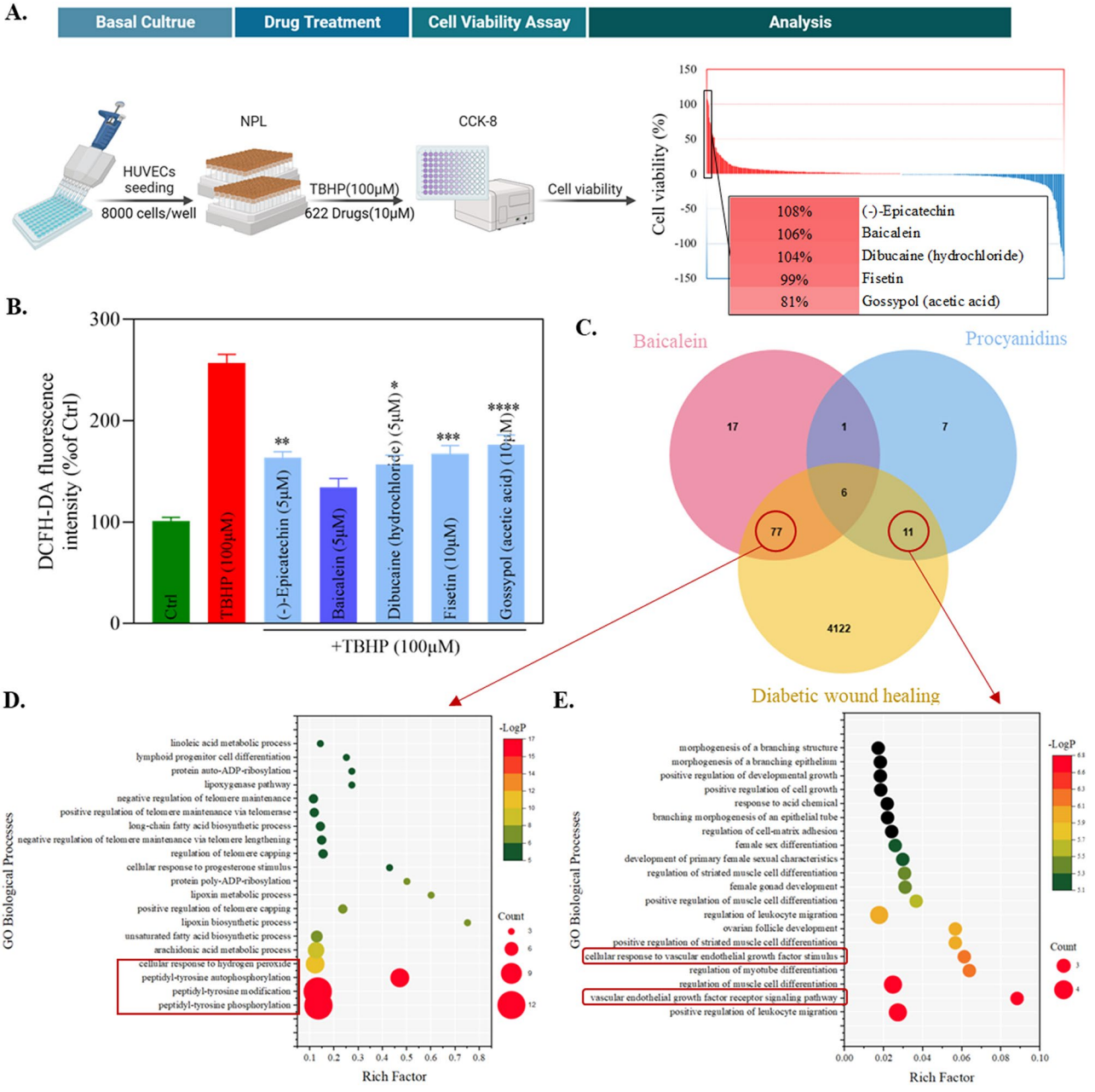

Fig. 2 High-throughput Drug Screening, Network Pharmacology, and GO Enrichment Analysis. (**A**) The process diagram and analytical outcomes of high-throughput drug screening in NPL. (**B**) Effects of different drugs with TBHP on ROS levels in HUVECs ($n = 3$). $^{*}P < 0.05$, $^{**}P < 0.01$, $^{***}P < 0.005$, $^{****}P < 0.001$, vs. that of Baicalein. (**C**) Venn diagram for the potential target of procyanidins and baicalein and the disease targets of diabetic wound healing. (**D**) Bubble chart of the biological process category terms from GO enrichment analysis for the 77 common targets. (**E**) Bubble chart of the biological process category terms from GO enrichment analysis for the 11 common targets

BPPNs (Fig. 3F). In summary, it can be inferred that in BPPNs, PC, and BAI can undergo proportional addition reaction to generate hemiketals, which are then connected by intermolecular forces to synthesize smaller-diameter polyphenol nanovesicles.

In order to further investigate the biological activity of PNs, toxicity tests were conducted on PNs (Figure S2 A and B). The maximum safe concentration for subsequent experiments was determined to be 4 μg/ml (After conversion, the content of BAI and PC in 4 μg/ml BPPNs is approximately 5 μM each). To facilitate the in vitro monitoring of the extracellular uptake of PNs, we employed the fluorescent dye FITC to label PNs. Under both conditions—with and without TBHP stimulation, cellular uptake of PNs was recorded at 1 h and 2 h (Fig. 3G). Quantitative results, as shown in Fig. 3H, reveal that

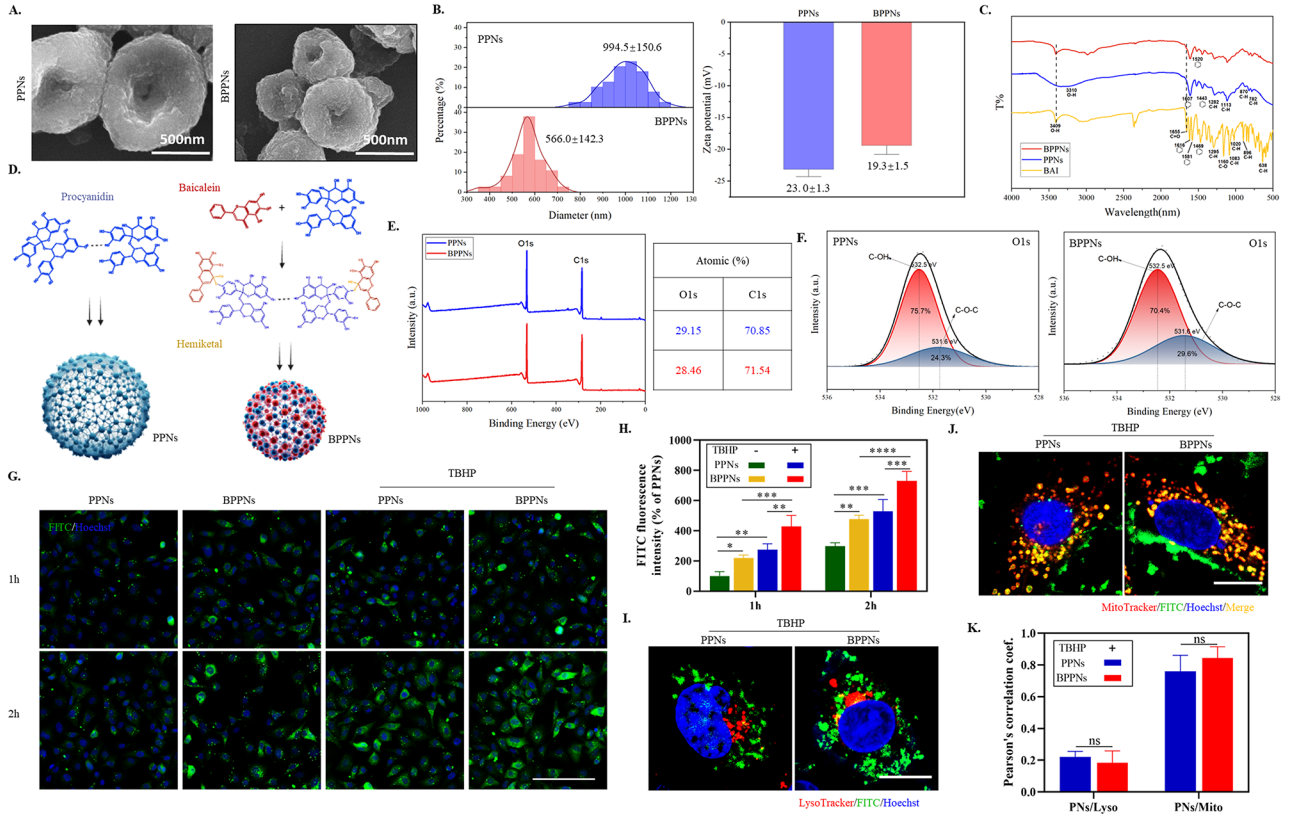

Fig. 3 The Synthesis and Characterization of PPNs and BPPNs. (**A**) SEM image of PPNs and BPPNs. Scale bar: 500 nm. (**B**) Particle size and Zeta potential of PPNs and BPPNs. (**C**) FTIR spectra of BAI, PPNs and BPPNs. (**D**) Schematic of PPNs and BPPNs synthesis. (**E**) XPS full spectrum of PPNs and BPPNs. (**F**) The high-resolution XPS spectrum for O1s of BPPNs. (**G**) Images of HUVECs taking up PPNs and BPPNs. Green: FITC-labeled PNs; Blue: Hoechst (nuclei). Scale bar: 100 μm. (**H**) Quantitative measurement of FITC fluorescence intensity in G. (**I**) Confocal microscope images locating FITC-labeled PPNs and BPPNs relative to lysosomes in HUVECs cells with TBHP. Green: FITC-labeled PNs; Red: LysoTracker (lysosome); Blue: Hoechst (nuclei). Scale bar: 10 μm. (**J**) Confocal microscope images locating FITC-labeled PPNs and BPPNs relative to mitochondrions in HUVECs cells with TBHP. Green: FITC-labeled PNs; Red: MitoTracker (mitochondrion); Blue: Hoechst (nuclei). Scale bar: 10 μm. K. Pearson's correlation coefficients indicating the degree of PNs/lysosome and PNs/Mitochondrion colocalization in I and J : $R=1$ (perfect colocalization), $R=0$ (no colocalization). $n=3$, $^{*}P<0.05$, $^{**}P<0.01$, $^{***}P<0.005$, $^{****}P<0.001$

both PPNs and BPPNs exhibit time-dependent and ROS-responsive uptake. Notably, BPPNs demonstrate a greater cellular uptake efficiency compared to PPNs, which may be attributed to the smaller size and increased ease of cellular internalization associated with BPPNs. After co-treatment with PNs and TBHP for two hours, the localization relationship between PNs and cellular organelles was assessed using LysoTracker and MitoTracker (Fig. 3I and J). The quantitative results of Pearson's correlation coefficient indicate that both types of vesicles can achieve lysosomal escape and co-localize with mitochondria under oxidative stress (Fig. 3K).

In summary, compared with PPNs, the newly synthesized BPPNs have been optimized in characterization. BPPNs are a novel type of polyphenolic nanovesicles with smaller particle size, higher cellular uptake efficiency, lysosomal escape, and mitochondrial ROS response properties.

In vitro angiogenic activity of BPPNs

Based on the network pharmacology and enrichment analysis results from Fig. 2C and E, it is speculated that PC may participate in or affect the VEGF signal pathway during the process of diabetes wound healing. In response to VEGF stimulation, endothelial cells sprout from the capillaries and then complete the entire process of angiogenesis with the proliferation, migration, and tubular formation of these cells, ultimately providing nutrients to the wound tissue, which is a key step in wound healing [1, 26].

To further clarify the impact of PNs on angiogenesis, we conducted relevant tests on HUVECs. Scratch assays were performed on attached HUVECs. Western blot results indicated that both BPPNs and PPNs effectively upregulated the expression of vascular angiogenesis-related proteins, including VEGF, and its upstream regulator HIF-1α (Fig. 4A, B). The cells were treated with BAI (5 μM), PPNs (4 μg/ml), or BPPNs (4 μg/ml) for 24 h, with HUVEC migration recorded at 0 h, 12 h, and

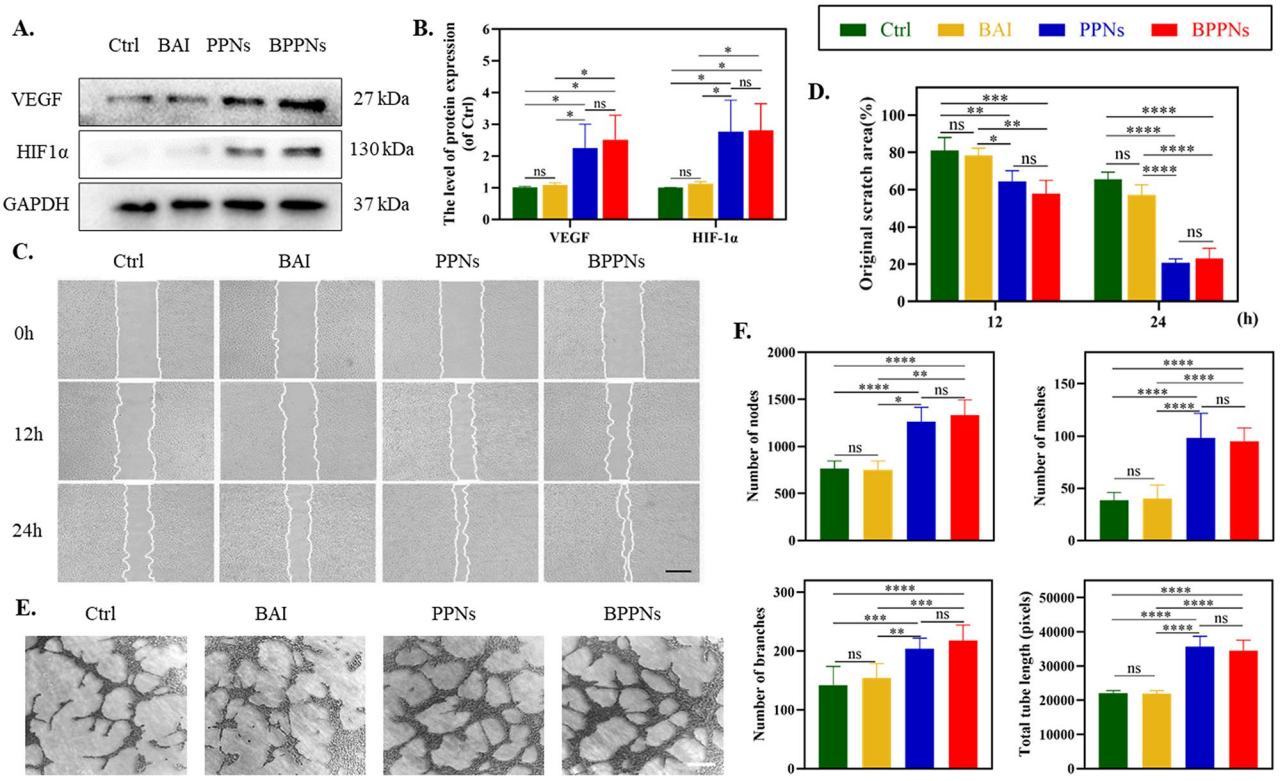

Fig. 4 The angiogenic properties of BPPNs in vitro. **A**-**B**. Western blots of VEGF and HIF-1α by HUVECs incubated in different preparations for 24 h. **C**. Representative images of HUVEC migration after treating for 0, 6, 12 h, scale bar: 500 μm. **D**. Quantify the migration of HUVEC. **E**. Representative images of HUVEC tubular formation after treating for 4 h, scale bar: 200 μm. **F**. Quantify the tubular formation of HUVEC. $n = 3$, $^{*}P < 0.05$, $^{**}P < 0.01$, $^{***}P < 0.005$, $^{****}P < 0.001$

24 h (Fig. 4C). The results reveal that, when compared to the control group, BAI exhibited no significant impact on HUVECs' migration. However, PPNs synthesized via PC significantly enhanced scratch healing. Notably, BPPNs containing BAI also have similar cell migration-promoting effects as PPNs (Fig. 4D). Following this, we performed tube formation assays on HUVECs from different treatment groups on the Matrigel matrix (Fig. 4E), and quantified the number of nodes, meshes, branches, and total tube length (Fig. 4F). The results demonstrated that BAI had almost no effect on the tube formation of HUVECs, while BPPNs exhibited a promotion of tube formation activity similar to that of PPNs. Overall, although BAI does not affect tube formation, BPPNs can effectively upregulate angiogenic-related proteins, promote the migration and tube formation of HUVECs, and obtain similar promoting tube activity as PPNs.

In vitro antioxidant activity of BPPNs

To further explore the in vitro antioxidant activity of BPPNs, HUVECs were divided into five groups as shown in Fig. 5, with a treatment duration of 24 h, and a series of tests were conducted. The CCK-8 results indicated that BAI, PPNs, and BPPNs could all mitigate the reduction in cell viability caused by TBHP, with the rescue effect increasing in the order of PPNs < BAI < BPPNs (Fig. 5A). Compared to the Ctrl group, the oxidative stress level in HUVECs of the TBHP group was significantly elevated (marked by a decrease in SOD activity and an increase in MDA content), while the antioxidative stress capabilities of PPNs, BAI, and BPPNs were enhanced (Fig. 5B). ROS probes and JC-1 staining were performed on HUVECs under different treatments (Fig. 5C and E). Oxidative stress induced by TBHP led to an increase in intracellular ROS and mitochondrial damage, with BPPNs showing the best capability in counteracting ROS and repairing mitochondrial damage, followed by BAI (Fig. 5D and F). Therefore, it is speculated that the prominent antioxidant activity of BPPNs is largely attributed to BAI, which was identified through high-throughput screening in the NPL.

Based on the outcomes of network pharmacology and enrichment analyses (Fig. 2C and D), it is hypothesized that the exceptional antioxidative efficacy of BAI may be attributable to its regulatory function on tyrosine phosphorylation. Protein phosphorylation modification, particularly prevalent and functionally paramount, occurs in over 30% of cellular proteins. Despite tyrosine phosphorylation modifications (P-Tyr) constituting less than 1% of all protein phosphorylation modifications, they play a

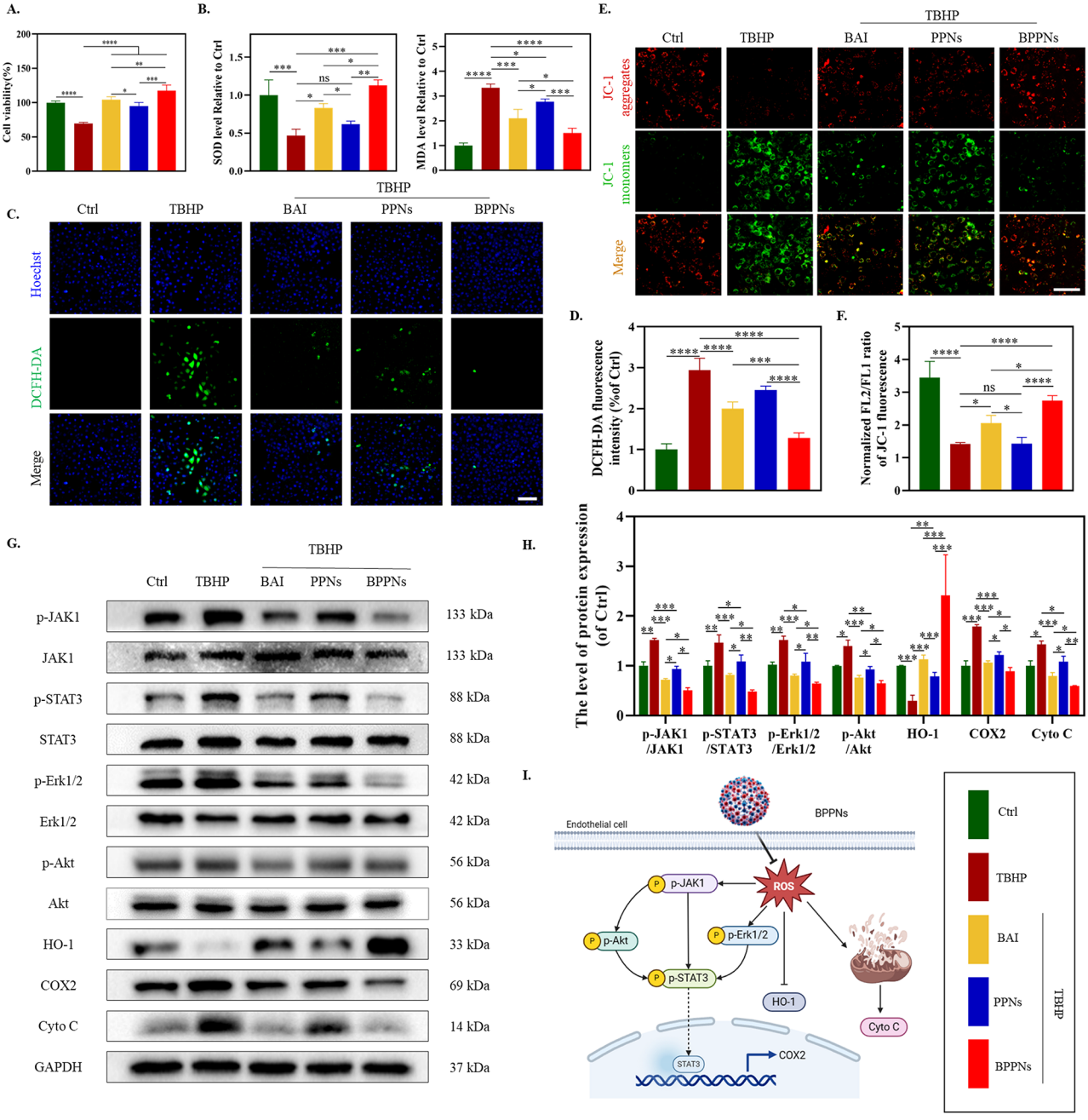

Fig. 5 In vitro antioxidant activity of BPPNs. (**A**) Effects of different preparations with TBHP on cell viability in HUVECs. (**B**) Effects of different preparations on SOD and MDA level in HUVECs. (**C**) DCFH-DA staining of HUVECs with different preparations. Scale bar: 100 μm. (**D**) Effects of different preparations on ROS levels in HUVECs. **E**-**F**. JC-1 staining images of HUVECs with different treatments. JC-1 aggregates: normal mitochondria (red); JC-1 monomers: unhealthy mitochondrial (green). Scale bar: 100 μm. **G**-**H**. Western blots of p-JAK1, JAK1, p-STAT3, STAT3, p-Erk1/2. Erk1/2, p-Akt, Akt, HO-1, COX2 and Cyto C by HUVECs incubated in different treatments. **I**. The antioxidant mechanism diagram of BPPNs. $n = 3$, $^{*}P < 0.05$, $^{**}P < 0.01$, $^{***}P < 0.005$, $^{****}P < 0.001$

pivotal role in nearly every physiological process within the cell [27, 28]. Studies have indicated that a high-fat diet in mice can affect the P-Tyr of liver proteins [29]. Proteins within pathways such as JAK1/STAT3 [30, 31], Erk1/2 [32], and Akt [33], all containing tyrosine residues, are subject to increased levels of tyrosine phosphorylation due to oxidative stress, thereby activating their respective signaling pathways. To validate the impact of BPPNs on P-Tyr and their antioxidative effects at the protein level, Western blot experiments were conducted (Fig. 5G). The results revealed that BAI significantly inhibits the tyrosine phosphorylation of pathway proteins JAK1, STAT3, Erk1/2, and Akt, markedly modulates oxidative stress-related proteins (upregulating HO-1 and downregulating

COX-2), and suppresses the expression of the mitochondria apoptosis-related protein Cyto C. These modulatory effects are notably superior to those of PPNs but inferior to those of BPPNs (Fig. 5H). Figure 5I was drawn based on the above experimental results and literature search [34, 35].

In summary, BPPNs can effectively counteract in vitro oxidative stress caused by TBHP by inhibiting tyrosine phosphorylation of pathway proteins, while also playing a role in mitochondrial protection (Fig. 5I).

BPPNs accelerate diabetic wound healing

In consideration of the application of PNs in diabetic wounds, we employed a photosensitive hydrogel with tissue adhesiveness, hyaluronic acid with o-nitrobenzene (HA-NB), to anchor the PNs at the wound sites [36, 37]. The establishment of a diabetic wound model in SD rats followed by the random allocation of these subjects into four groups, as depicted in Fig. 6. Initially, we evaluated the impact of treatments with HA-NB, PPNs@HA-NB, and BPPNs@HA-NB on the principal organs—heart, liver, spleen, lungs, and kidneys—through H&E staining of organ tissue sections. The absence of pathological alterations in these stained sections suggests that HA-NB, PPNs@HA-NB, and BPPNs@HA-NB do not exhibit organ toxicity, as illustrated in Supplementary Fig. 3.

Figure 6A and B depict the wound healing progression over fourteen days across four treatment groups, accompanied by a quantification of the wound areas (Fig. 6C). Compared to the DM group, the application of HA-NB significantly enhances the healing of diabetic wounds, likely attributable to the reduced risk of infection at the diabetic wound sites facilitated by the coverage provided by HA-NB [37]. It is particularly noteworthy that the BPPNs@HA-NB group exhibited a higher rate of diabetic wound healing compared to the PPNs@HA-NB group. Furthermore, we employed laser Doppler scan images to characterize the functional vasculature with blood flow (Fig. 6D). It was observed that BPPNs@HA-NB could effectively upregulate angiogenesis around the wound during the proliferative phase of healing, thereby abbreviating the prolonged proliferative phase induced by diabetes (Fig. 6E). Subsequent histopathological evaluation of the neo tissue on day 14 post-injury using H&E and Masson's trichrome staining is presented in Fig. 6F. Quantitative analyses, as shown in Fig. 6G, revealed that diabetic wound tissues treated with BPPNs@HA-NB had thicker granulation tissue, shorter wound lengths, and higher collagen deposition compared to the PPNs@HA-NB group. These findings collectively suggest that BPPNs significantly accelerate diabetic wound healing and promote the progression of wound healing processes in diabetes, in comparison to PPNs.

To investigate the intrinsic mechanisms underlying the therapeutic efficacy of BPPNs in treating of diabetic wounds, we further assessed the levels of oxidative stress, angiogenesis, and collagen within the tissue 14 days post-injury. The detection results for Superoxide Dismutase (SOD) and Malondialdehyde (MDA) indicated that the BPPNs@HA-NB group significantly reduced oxidative stress levels in diabetic wound tissues compared to the other three groups (Fig. 7A). Immunofluorescence co-staining for CD31 and α-SMA, markers of neovascularization (Fig. 7B), along with the quantification of fluorescence expression shown in Fig. 7C, demonstrated that the vascular density in the BPPNs@HA-NB group was comparatively higher. As depicted in Fig. 7D, immunohistochemical analysis of oxidative stress-related markers (COX2 and HO-1), mitochondrial apoptosis markers (Cyto C), angiogenesis-related markers (VEGF), and Collagen III (COL3) revealed that BPPNs@HA-NB could downregulate COX2 and Cyto C protein expression and upregulate the relative expression of HO-1, VEGF, and COL3 compared to the other three groups. These findings suggest that BPPNs may accelerate diabetic wound healing by counteracting oxidative stress, protecting mitochondria, promoting angiogenesis, and enhancing collagen deposition.

In summary, the newly synthesized polyphenol vesicles, BPPNs, optimized with BAI, demonstrate enhanced efficacy in counteracting the excessive oxidative stress encountered during diabetic wound healing compared to the original anthocyanin polyphenol vesicles, PPNs. Additionally, BPPNs retain the angiogenic-promoting effects of PPNs while their superior antioxidant activity creates a more "fertile ground" for angiogenesis. Consequently, the results indicate that BPPNs exhibit enhanced in vivo angiogenesis promotion compared to PPNs. Overall, BPPNs accelerate diabetic wound healing through a dual approach: combating oxidative stress and promoting angiogenesis, highlighting their potential as a multifaceted therapeutic intervention in diabetic wound management (Graphical abstract).

Discussion

In this study, we first assessed the level of oxidative stress during diabetic wound healing, confirming that diabetes leads to a sustained high level of oxidative stress in the peri-wound tissue, consistent with existing reports [7]. To explore further, we induced oxidative stress in HUVECs in vitro and conducted high-throughput screening of over six hundred compounds from the Natural Product Library, identifying BAI as the most effective antioxidant drug in endothelial cells. By combining BAI with the polyphenol vesicle framework material PC, in a 1:1 ratio and utilizing the physical adsorption properties of CaCO3, we synthesized a new nanovesicle,

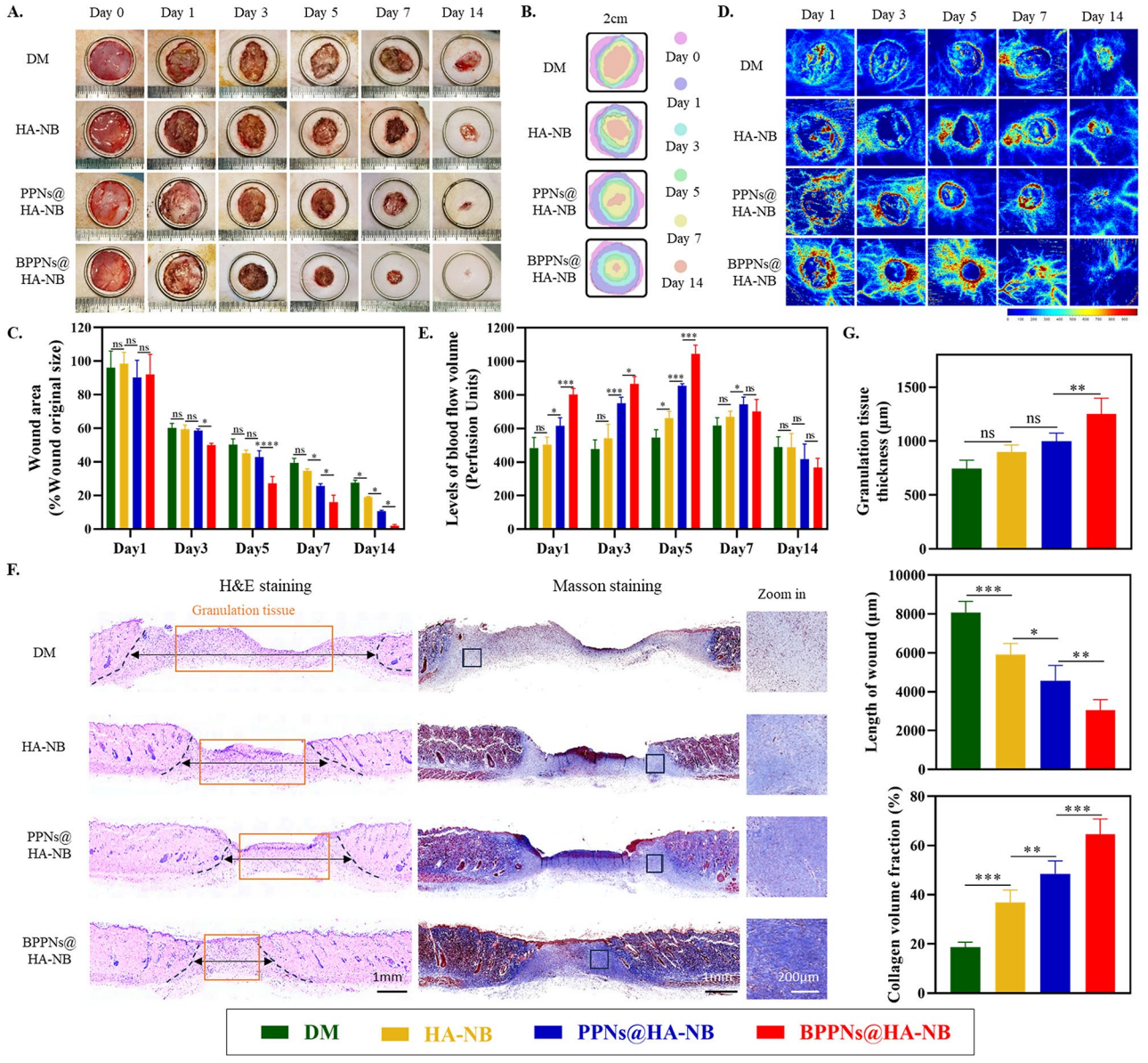

Fig. 6 In vivo evaluation of BPPNs in the diabetic rat full-thickness wounds model. (**A**) Representative photographic images of the wounds healing process with different treatments on day 0, 1, 3, 5, 7 and 14. (**B**) Traces of wound-bed closure during 14 days for each treatment. (**C**) percentage of wound area after treatment with the different preparations on day 1, 3, 5, 7 and 14. (**D**) Representative Laser Doppler scan images on the diabetic wound after treatment on day 0, 1, 3, 5, 7 and 14. (**E**) Quantification of blood flow volume at day 1, 3, 5, 7 and 14 using moorLDI Review V6.1 software. (**F**) H&E and masson staining evaluation of wound regeneration after treatment with the different preparations on the 14th day. The black dashed line show the border between the wound tissue and surrounding healthy skin tissue. (**G**) Quantification of granulation tissue thicknesses, the length of wound and collagen volume fraction for different treatments on the 14th day. $n = 5$, $^{*}P < 0.05$, $^{**}P < 0.01$, $^{***}P < 0.005$

BPPNs. Chemical analysis revealed that BAI forms a hemiketal with PC, creating a network structure through intermolecular forces, which we confirmed via FTIR and XPS. The incorporation of BAI into BPPNs results in smaller particle sizes compared to PPNs, enhancing cellular uptake efficiency. Additionally, BPPNs demonstrated ROS responsiveness and lysosomal escape capabilities, with co-localization with mitochondria under oxidative stress conditions. Network pharmacology and GO enrichment analysis suggest that PC may facilitate diabetic wound healing by influencing the VEGF signaling pathway, while BAI could impact protein tyrosine phosphorylation and cellular responses to hydrogen peroxide. We further investigated the bioactivity of BPPNs, We further investigated the bioactivity of BPPNs, finding that while BAI alone does not promote angiogenesis in HUVECs, both PPNs and BPPNs significantly enhance in vitro tube formation and upregulate VEGF expression.

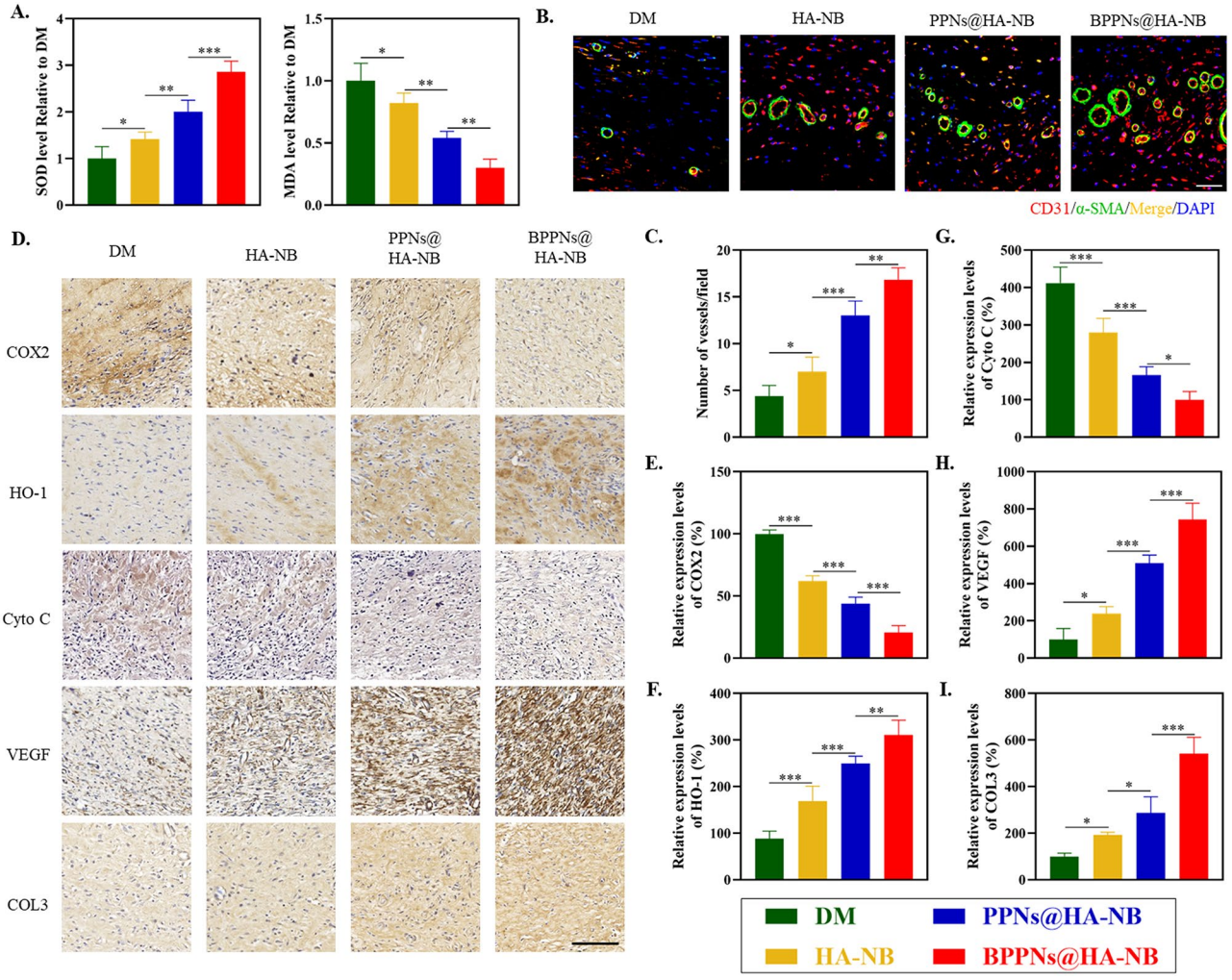

Fig. 7 Evaluation of the therapeutic efficacy after BPPNs treatment. (**A**) Effects of different preparations on SOD and MDA level on day 14. (**B**) Immunofluorescence staining of neovascularizationat the wound tissue with different treatments on day 14. α-SMA (green), CD31 (red), and DAPI (blue). Scale bar: 100 μm. (**C**) Quantitative analysis of the blood vessel density on day 14. (**D**) Corresponding immunohistochemistry staining of COX2, HO-1, Cyto C, VEGF and COL3 on day 14. Scale bar: 200 μm. **E**-**I**. Immunohistochemical quantification of COX2, HO-1, HIF-1α, VEGF and COL3, respectively. $n = 5$, $^{*}P < 0.05$, $^{**}P < 0.01$, $^{***}P < 0.005$

Under TBHP stimulation, BPPNs effectively inhibit pathway protein tyrosine phosphorylation, counteract oxidative stress, and facilitate mitochondrial repair, demonstrating a combined bioactivity of BAI and PPNs. In vivo studies confirm that BPPNs exhibit both angiogenic and antioxidative stress activities, significantly accelerating diabetic wound healing.

Diabetes is a chronic disease that poses a significant threat to global health, affecting over 500 million individuals affected globally by 2021, with incidence rates rising annually [38]. A defining characteristic of diabetes is elevated blood glucose levels, which over time can lead to oxidative stress, exacerbating hypoxia, inflammation, and cellular apoptosis [39]. These conditions contribute to most diabetic complications. Among these, diabetic wounds are particularly concerning due to their non-healing nature, which can results in ulcers and even amputation [40]. Research indicates that the persistence of non-healing wounds in diabetic patients is primarily due to excessive oxidative stress in the peri-wound tissue and a diminished antioxidant capacity following the onset of diabetes [3]. Thus, this article aims to develop an effective antioxidant treatment strategy that targets oxidative stress during the diabetic wound healing process.

The onset and progression of oxidative stress primarily arise from the generation of ROS and distruptions in signaling pathways [41, 42]. ROS can induce these signaling pathway aberrations, further exacerbating ROS production. Consequently, antioxidant therapy can be broadly categorized into two approaches: chemical removal of peroxides through direct chemical reactions and the modulation of signaling pathways through biological

means [7]. A dual approach is essential for effectively mitigating oxidative stress. From a chemical perspective, the scaffold used in this study, PC, contains numerous phenolic hydroxyl groups, which theoretically enable it to counteract oxidative stress by reacting directly with ROS. Literature also suggests that PC can serve as a protective barrier against oxidative stress by reducing the burden of free radicals, thereby preventing molecular and cellular damage [43]. In this research, PPNs formed through physical adsorption and intermolecular forces of PC, exhibit ROS responsiveness and demonstrate antioxidative activity both in vitro and in vivo (Figs. 5 and 7). However, their impact on pathway proteins and overall antioxidative efficacy is relatively modest, suggesting that the antioxidative activity of PC primarily derives from its chemical structure. Therefore, optimizing PPNs is crucial for enhancing their antioxidative properties.

Natural products are valued for their high biological activity, low toxicity, and significant potential for development, attracting considerable attention from clinicians and researchers. Consequently, our focus has shifted to this area. Through high-throughput screening of the natural product library under oxidative stress conditions, BAI emerged as a standout candidate owing to its remarkable antioxidative activity. Interestingly, BAI contains a polyphenolic structure; however, its phenolic hydroxyl is considerably lower than that of PC. At a result, from a chemical perspective, BAI's ability to directly react with ROS is presumed to be inferior to that of PC. Thus, we hypothesize that BAI primarily combats oxidative stress by modulating signaling pathways. Subsequent network pharmacological analysis validated this hypothesis (Fig. 2C and D), indicating that BAI influences protein tyrosine phosphorylation across multiple GO biological processes. To further validate this, we selectively screened several pathway proteins closely associated with oxidative stress and harboring tyrosine residues, including JAK1, STAT3, Erk1/2, and Akt. Western blot results (Figures G and H) revealed that BAI effectively inhibits the phosphorylation of these pathway proteins, ultimately yielding antioxidative stress and mitochondrial damage repair effects. BPPNs, BAI-optimized polyphenol nanovesicles, unsurprisingly, exhibited superior antioxidative activity both in vitro and in vivo (Figs. 5 and 7), highlighting the effectiveness of a dual antioxidative strategy involving both chemical and biological pathways.

It's noteworthy that in network pharmacology analysis, PC and BAI have non-overlapping targets with the common related to diabetic wounds, addressing two key aspects of treatment: angiogenesis and oxidative stress. The angiogenesis-promoting effect of PC has been verified in both in vivo and in vitro experiments, endowing BPPNs with angiogenic activity that BAI lacks. Therefore, the synthesis of BPPNs not only combines the antioxidative activities of PC and BAI but also achieves a complementary functional effect.

Nanoparticles (NPs) are commonly used as part of drug delivery systems due to their ability to enhance pharmacokinetics, bioavailability, and the half-life of drug formulations, while also reducing the frequency of dosing for gene or drug molecules [44]. Given the amphiphilic and network structure of BPPNs, it's reasonable to speculate that the polyphenol vesicles can also carry drugs or transport exogenous proteins, amino acids, or even nucleic acid sequences into cells. Coupled with their inherent biological activity, this could potentially achieve therapeutic effects that improve disease outcomes. However, further development and optimization are necessary to fully realize this potential.

In summary, this study utilized high-throughput screening of a natural product library to identify BAI as the most effective antioxidant in HUVECs. By leveraging the biological activity and chemical structure of BAI, we characterized and functionally optimized PPNs, resulting in BPPNs with smaller particle size, faster cellular uptake, and stronger ROS response. These vesicles accelerate diabetic wound healing by simultaneously combating oxidative stress and promoting angiogenesis.

Conclusion

In this study, we synthesized and successfully validated a multifunctional polyphenol nanoparticle vesicle, BPPNs, optimized through natural products, targeting excessive oxidative stress during the healing process of diabetic wounds. Through screening the antioxidant activity of over six hundred natural products from the natural product library, baicalin was selected for its optimal antioxidant stress effect in HVECs. Baicalin undergoes an additive reaction with the polyphenol biomaterial Procyanidins, utilizing intermolecular forces to form BPPNs, which accelerate cellular uptake under oxidative stress conditions and exhibit the biological activities of baicalin and proanthocyanidins intracellularly. BPPNs not only exert antioxidant activity by inhibiting the phosphorylation of pathway proteins such as tyrosine but also accelerate diabetic wound healing by further promoting angiogenesis and collagen deposition. Overall, our research results offer a new therapeutic strategy for the healing of diabetic wounds.

Experimental Section/methods

Reagents and kits

Natural Product Library (#HY-L021) and FluoroTag™ FITC Conjugation Kit (#HY-66019) from MedChemexpress (NJ, USA). Fetal bovine serum (FBS, #10099141 C) was obtained from Gibco-Invitrogen (NY, USA). Dulbecco's Modified Eagle Medium (DMEM, #MA0212),

Penicillin/Streptomycin, sterile(100X) (#MA0110), phosphate buffered solution (PBS, #MA0015), 0.25%Trypsin-EDTA, PhenolRed(modified) (#PWL060), Streptozotocin (STZ, #MB1227), Procyanidins (#MB2168-1), Baicalein (#MB7311) and other reagents required for cell culture were obtained from Meilunbio (Dalian, China). High-fat feed (#MD12033) purchased from Medicience (Jiangsu, China). Tert-butyl hydroperoxide solution (TBHP, #418064) and DMSO (#D2650) were purchased from Sigma-Aldrich (St Louis, MO, USA). Cell Counting Kit-8 (#C0040), Protease inhibitor cocktail for general use (#P1005), SDS-PAGE Sample Loading Buffer (5X) (#P0015), Enhanced BCA Protein Assay Kit (#P0010), Hoechst 33,258 (#C1011) and BeyoECL Star (#P0018AM) were purchased from Beyotime (Shanghai, China). 2′,7′-Dichlorofluorescin diacetate (DCFH-DA, #D6470), Superoxide Dismutase (SOD) Activity Assay Kit (#BC0175), Malondialdehyde (MDA) Content Assay Kit (#BC0025), Mitochondrial Membrane Potential Assay Kit with JC-1 (#M8650), Hematoxylin-Eosin (HE) Stain Kit (#G1120), Masson's Trichrome Stain Kit (#G1340), DAB Substrate kit (20×) (#DA1010), Mounting Medium (antifading, with DAPI) (#S2110) and were purchased from Solarbio Science & Technology (Beijing, China). MitoTracker™ Red CMXRos (#M7512) and LysoTracker™ Deep Red (#L12492) were purchased from Thermo Fisher Scientific Inc. (Waltham, MA, USA). Goat Anti-Mouse IgG H&L (Alexa Fluor® 488) (#ab150113), and Goat Anti-Rabbit IgG H&L (Alexa Fluor® 594) (#ab150080) were purchased from Abcam (Cambridge, UK) (Table 1).

Animal model of diabetic full-thickness wounds

All animal experiments were approved by the Institutional Ethical Committee of Wenzhou Medical University (wydw2023-0243). The Experimental Animal Center of Wenzhou Medical University (Zhejiang Province, China) provided a total of 40 male 6-week-old SD rats (180–220 g). After adaptive feeding for 1 week, high-fat diets were given for 4 weeks. Intraperitoneal injections were administered for 3 days each time: 60 mg/kg STZ (T2D, $n=30$) until blood glucose stabilizes > 16.67mmol/L; 0.25 ml/kg 0.9% NaCl (Ctrl, $n=10$). Continue high-fat feeding for 4 weeks.

For the wounds model, animals were anesthetized with 2.5% pentobarbital sodium (30 mg/kg) and randomly selected for grouping. After shaving and sterilization, two full-thickness wounds (20 mm in diameter) were made by scissor cutting along the mark on each side of the rat's back. All the animals were high-fat fed in individual cages and given ad libitum feeding access to food and water, and they were observed every day during the total period of the experiment. At days 0, 1, 3, 5, 7, 14, and 21 post-treatment, the wound area was calculated by tracing the wound margins from rats and was evaluated as a percent area of the original wound using Image J software.

Table 1 Primary antibodies were used in the study

Antibody	Purpose	Product ID and manufacturer
p-JAK1	WB	#741,295, Cell Signaling Technology, USA
JAK1	WB	#66,466, Proteintech, China
p-STAT3	WB	#9145, Cell Signaling Technology, USA
STAT3	WB	#12,640, Cell Signaling Technology, USA
COX2	WB/ IHC	#12,282, Cell Signaling Technology, USA
HO-1	WB/ IHC	#10701-1-AP, Proteintech, China
Cyto C	WB/ IHC	#10993-1-AP, Proteintech, China
VEGF	WB/ IHC	#ET1604-28, Huabio, China
HIF-1α	WB	#66,730, Proteintech, China
CD31	IF	#ab281583, Abcam, UK
α-SMA	IF	#BM0002, Boster, China
COL3	IHC	#ER1906-50, Huabio, China
GAPDH	WB	#2118, Cell Signaling Technology, USA

High-throughput screening of natural product library

Using human umbilical vein endothelial cells (HUVECs) to screen 622 drugs from the natural product library. HUVECs were seeded into a 96-well plate (8000 cells/well) and cultured for 24 h until they adhered to the walls. A blank control group, stimulation group (TBHP 100μM), and drug treatment group (TBHP 100μM + drug 10μM) were set up in the plate, and after 24 h of treatment, the detection was performed using CCK8, measuring absorbance at a wavelength of 450 nm with an enzyme reader, designated as Ac, Ab, and As, respectively. Cell viability was calculated for each drug treatment using the formula and subjected to statistical analysis ($n=3$).

$$Cell\ viability\,(\%) = \frac{As - Ab}{Ac - Ab} \times 100\%$$

Network pharmacology and GO biological processes enrichment analysis

The two-dimensional conformations of Procyanidins and baicalein were downloaded from PubChem's official website (https://pubchem.ncbi.nlm.nih.gov/). Isomeric Smiles format files were imported into the Swiss Target Prediction (http://swisstargetprediction.ch/) platform, set the attribute to Homo sapiens, and start to predict the potential target of Procyanidins and baicalein. By searching the keyword of diabetic wound healing in the GeneCards (https://www.genecards.org/) database to obtain the disease targets. Compare the three datasets mentioned above by creating a Venn diagram (https://jvenn.toulouse.inrae.fr/app/index.html), and performing an enrichment analysis of GO biological processes on the genes at the intersection (https://metascape.org/gp/index.html).

Preparation and characterization of PPNs and BPPNs

After adding 1 mL of 1 M Na_2CO_3 solution to a 15 mL conical flask and stirring at 1200 rpm, 1 mL of ddH_2O is added. Then, 0.5 mL 10mM Procyanidins and baicalein are added to the conical flask. Stirring continues, and 1 mL of 1 M $CaCl_2$ solution is added. Stirring is continued. After allowing it to stand for 15 min, the mixture is centrifuged at 1000 rpm and washed with water three times. The washed samples are then mixed with 4 mL of 1 M HCl and centrifuged at 3000 rpm until the pH is between 6 and 6.5. Afterward, freeze-drying is performed to obtain BPPNs. As for PPNs, repeat the above process by replacing the baicalein solution with an equimolar solution of Procyanidins. The freeze-dried powder was dissolved and diluted in DMEM to prepare vesicle solutions at different concentrations.

The morphology of nanoparticles was observed by scanning electron microscopy (SEM) (Quanta 250 FEG, FEI). The particle size and Zeta potential analyses of nanoparticles were carried out on the Malvern Zetasizer Nano ZS (Malvern Instruments, UK). Chemical interaction between NA was recorded on a Nicolet IS10 FT-IR instrument (ThermoFisher Scientific, USA) scanning from 4000 to 500 cm^{-1}. XPS was measured by ESCALAB 250Xi K-alpha (ThermoFisher Scientific, USA).

For BPPNs:

$$\begin{aligned} &C1s/O1s = (71.54\%)\,/\,(28.46\%) \\ &= (30PC + 15BAI)\,/\,(13PC + 5BAI) \\ &\rightarrow PC/BAI \approx 1 \end{aligned}$$

Western blot

HUVECs were subjected to a 1:4 dilution with a 5X loading buffer and subsequently exposed to a heat treatment at 100 °C for 15 min. The resultant protein extracts were then resolved through a 12.5% SDS-PAGE gel and transferred onto PVDF membranes. Following this, the membranes were subjected to a blocking procedure involving 5% nonfat milk for 2 h. After the milk blocking, the membranes underwent a series of washes using TBST and were subsequently incubated with primary antibodies for 8–12 h at 4 °C. Following this primary antibody incubation, the membranes were once again subjected to TBST washes and subsequently incubated with secondary antibodies conjugated with HRP for 2 h at RT. The visualization of immunoreactive bands was achieved through the utilization of an ECL kit and the bands were detected using a ChemiDoc Imaging System (Bio-Rad, USA).

In vitro tube formation assay

A tube formation assay using Matrigel® matrix (#356234, Corning, USA) was conducted to assess the morphogenesis and tube formation capability of HUVECs under different treatments. In brief, the Matrigel solution was allowed to thaw at 4 °C overnight and subsequently dispensed into μ-Slide chambers (10 μL per well, IBIDI, Germany), followed by incubation in a cell incubator for 1 h to facilitate solidification. A total of 5000 cells, which had been pre-treated with BAI (10μM), PPNs, and BPPNs, were seeded onto the Matrigel-precoated μ-Slide. Tube formation was meticulously observed and quantified, with an average count derived from the assessment of three independent fields, all conducted under an inverted light microscope (Olympus, Japan).

Scratch-wound healing assay

Cultivate HUVECs in a 6-well culture plate until they adhere to the walls. Scratch the cell surface gently using the tip of a sterile 200-μL pipette. Remove floating cells with PBS and continue with a complete culture medium containing 5% FBS. Capture images of the scratches at 0 h, 12 h, and 24 h, respectively, under an inverted microscope.

Assessment of blood flow in the wound area

The blood flow in the wound area was assessed by a laser Doppler imager (MoorLDI-2; Moor Instruments Limited, Devon, UK). Briefly, the rats were anesthetized with 2.5% pentobarbital sodium (30 mg/kg), shaved, and then gently fixed onto a black platform. MoorLDI Review V6.1 software was used to quantify the results.

Histology analysis and immunohistochemistry

On the 14th day, the rats were perfused with physiological saline. The wound was fixed with 4% paraformaldehyde at 4 °C, followed by paraffin embedding. The embedded tissues were sectioned and stained with hematoxylin and eosin (H&E) as well as Masson's trichrome stain to assess inflammation, epidermal regeneration, granulation tissue, and collagen deposition. Immunohistochemistry and immunofluorescence were performed to evaluate the expression of various markers.

Statistical analysis

Numerical data, presented as mean values accompanied by their respective standard deviations (mean ± SD), are depicted based on the results of a minimum of three distinct experiments unless stated otherwise. Statistical analysis of the data was conducted through a one-way analysis of variance (ANOVA), followed by Tukey's post-hoc analysis, utilizing GraphPad Prism 7.0 (La Jolla, CA, USA). Statistical significance was established at a threshold of $P<0.05$, and comparisons were made at two significance levels, $^{*}P<0.05$, $^{**}P<0.01$, $^{***}P<0.005$, $^{****}P<0.001$ against the specified reference group.

Supplementary Information

The online version contains supplementary material available at https://doi.org/10.1186/s12951-024-02950-2.

Supplementary Material 1

Acknowledgements
The authors thank Professor Linyong Zhu from the school of Biomedical engineering, Shanghai Jiao Tong University, for providing us with HA-NB hydrogel. This study was supported by Zhejiang Provincial Natural Science Foundation of China (LY22H060008).

Author contributions
XY. Zhao: Writing – original draft, Methodology, Formal analysis, Conceptualization. SK Su: Methodology. CY. Wu: Methodology, Formal analysis. YX. Deng: Methodology. Y. Chen: Methodology. TX. Yu: Methodology. CC. Li: Methodology. YK. Zhang: Methodology. XY. Wang: Project administration. YF. Zhou: Funding acquisition. XL. Zhang: Writing – review & editing, Methodology, Formal analysis. All authors have read and approved the content of the manuscript.

Data availability
All animal experiments were approved by the Institutional Ethical Committee of Wenzhou Medical University (wydw2023-0243).

Declarations

Ethics approval and consent to participate
All animal experiments were approved by the Institutional Ethical Committee of Wenzhou Medical University (wydw2023-0243).

Consent for publication
Not applicable.

Competing interests
The authors declare no competing interests.

Author details
[1]Department of Orthopaedics, The Second Affiliated Hospital and Yuying Children's Hospital of Wenzhou Medical University, Wenzhou, Zhejiang Province, China
[2]Zhejiang Provincial Key Laboratory of Orthopedics, Wenzhou, Zhejiang Province, China
[3]The Second School of Medicine, Wenzhou Medical University, Wenzhou, Zhejiang Province, China

Received: 21 August 2024 / Accepted: 22 October 2024
Published online: 21 November 2024

References

1. Rodrigues M, et al. Wound Healing: a Cellular Perspective. Physiol Rev. 2019;99(1):665–706. https://doi.org/10.1152/physrev.00067.2017.
2. Chen L, et al. The role of antioxidants in photoprotection: a critical review. J Am Acad Dermatol. 2012;67(5):1013–24. https://doi.org/10.1016/j.jaad.2012.02.009.
3. Cano Sanchez M, et al. Targeting oxidative stress and mitochondrial dysfunction in the treatment of impaired Wound Healing: a systematic review. Antioxid (Basel). 2018;7(8). https://doi.org/10.3390/antiox7080098.
4. Dunnill C, et al. Reactive oxygen species (ROS) and wound healing: the functional role of ROS and emerging ROS-modulating technologies for augmentation of the healing process. Int Wound J. 2017;14(1):89–96. https://doi.org/10.1111/iwj.12557.
5. Wang G, et al. The initiation of oxidative stress and therapeutic strategies in wound healing. Biomed Pharmacother. 2023;157:114004. https://doi.org/10.1016/j.biopha.2022.114004.
6. Monaghan MG, et al. Thou shall not heal: overcoming the non-healing behaviour of diabetic foot ulcers by engineering the inflammatory microenvironment. Adv Drug Deliv Rev. 2023;203:115120. https://doi.org/10.1016/j.addr.2023.115120.
7. Forman HJ, Zhang H. Targeting oxidative stress in disease: promise and limitations of antioxidant therapy. Nat Rev Drug Discov. 2021;20(9):689–709. https://doi.org/10.1038/s41573-021-00233-1.
8. Schaper NC, et al. Prevention and management of foot problems in diabetes: a Summary Guidance for Daily Practice 2015, based on the IWGDF guidance documents. Diabetes Res Clin Pract. 2017;124:84–92. https://doi.org/10.1016/j.diabres.2016.12.007.
9. Chen L, et al. Adipose-derived stem cells promote diabetic wound healing via the recruitment and differentiation of endothelial progenitor cells into endothelial cells mediated by the VEGF-PLCgamma-ERK pathway. Arch Biochem Biophys. 2020;692:108531. https://doi.org/10.1016/j.abb.2020.108531.
10. Liang Y, et al. pH/Glucose dual responsive Metformin Release Hydrogel dressings with Adhesion and Self-Healing via Dual-dynamic bonding for athletic Diabetic Foot Wound Healing. ACS Nano. 2022;16(2):3194–207. https://doi.org/10.1021/acsnano.1c11040.
11. Wang H, et al. Natural polyphenols in drug delivery systems: current status and future challenges. Giant. 2020;3. https://doi.org/10.1016/j.giant.2020.100022.
12. Li N, et al. Subtle distinction in molecular structure of flavonoids leads to vastly different coating efficiency and mechanism of metal-polyphenol networks with excellent antioxidant activities. Colloids Surf B Biointerfaces. 2023;229:113454. https://doi.org/10.1016/j.colsurfb.2023.113454.
13. Chen M, et al. Natural carrier-free self-assembled diterpene nanoparticles with its efficient anti-inflammation through the inhibition of NF-kappaB pathway for accelerated wound healing. Biomed Pharmacother. 2023;165:115041. https://doi.org/10.1016/j.biopha.2023.115041.
14. Lu YC, et al. Augmented cellular uptake of nanoparticles using tea catechins: effect of surface modification on nanoparticle-cell interaction. Nanoscale. 2014;6(17):10297–306. https://doi.org/10.1039/c4nr00617h.
15. Untener EA, et al. Tannic acid coated gold nanorods demonstrate a distinctive form of endosomal uptake and unique distribution within cells. ACS Appl Mater Interfaces. 2013;5(17):8366–73. https://doi.org/10.1021/am402848q.
16. Yuan T, et al. Robust and multifunctional nanoparticles assembled from natural polyphenols and metformin for efficient spinal cord regeneration. ACS Nano. 2023;17(18):18562–75. https://doi.org/10.1021/acsnano.3c06991.
17. Devi LM, et al. Effect of gelatin and acacia gum on anthocyanin coacervated microcapsules using double emulsion and its characterization. Int J Biol Macromol. 2023;235:123896. https://doi.org/10.1016/j.ijbiomac.2023.123896.
18. Fu Z, et al. Recent development of carrier materials in anthocyanins encapsulation applications: a comprehensive literature review. Food Chem. 2024;439:138104. https://doi.org/10.1016/j.foodchem.2023.138104.
19. Liu HM, et al. Possible mechanisms of oxidative stress-Induced skin Cellular Senescence, inflammation, and Cancer and the therapeutic potential of Plant Polyphenols. Int J Mol Sci. 2023;24(4). https://doi.org/10.3390/ijms24043755.
20. Neilson AP, et al. High-molecular-weight proanthocyanidins in Foods: overcoming Analytical challenges in Pursuit of Novel Dietary Bioactive Components. Annu Rev Food Sci Technol. 2016;7:43–64. https://doi.org/10.1146/annurev-food-022814-015604.
21. Huang S, et al. Size-controllable food-grade nanoparticles based on sea cucumber polypeptide with good anti-oxidative capacity to prolong lifespan in tumor-bearing mice. Int J Biol Macromol. 2023;253:127039. https://doi.org/10.1016/j.ijbiomac.2023.127039.
22. Han Y, et al. Ferrous ions doped calcium carbonate nanoparticles potentiate chemotherapy by inducing ferroptosis. J Control Release. 2022;348:346–56. https://doi.org/10.1016/j.jconrel.2022.06.002.
23. Cai Z, et al. Mussel-inspired pH-Switched assembly of capsules with an ultrathin and Robust Nanoshell. ACS Appl Mater Interfaces. 2019;11(31):28228–35. https://doi.org/10.1021/acsami.9b11445.
24. Yin Y, et al. Controlled self-assembly of natural polyphenols driven by multiple molecular interactions. ChemPlusChem. 2024;89(5):e202300695. https://doi.org/10.1002/cplu.202300695.
25. Zhu S, et al. Microenvironment responsive nanocomposite hydrogel with NIR photothermal therapy, vascularization and anti-inflammation for diabetic infected wound healing. Bioact Mater. 2023;26:306–20. https://doi.org/10.1016/j.bioactmat.2023.03.005.
26. Liu K, et al. Redox Modulatory Cu(II)-Baicalein Microflowers prepared in one step effectively promote therapeutic angiogenesis in Diabetic mice. Adv Healthc Mater. 2022;e2202010. https://doi.org/10.1002/adhm.202202010.

27. Sharma K, et al. Ultradeep human phosphoproteome reveals a distinct regulatory nature of Tyr and Ser/Thr-based signaling. Cell Rep. 2014;8(5):1583–94. https://doi.org/10.1016/j.celrep.2014.07.036.
28. Hunter T. Tyrosine phosphorylation: thirty years and counting. Curr Opin Cell Biol. 2009;21(2):140–6. https://doi.org/10.1016/j.ceb.2009.01.028.
29. Dittmann A, et al. High-fat diet in a mouse insulin-resistant model induces widespread rewiring of the phosphotyrosine signaling network. Mol Syst Biol. 2019;15(8):e8849. https://doi.org/10.15252/msb.20198849.
30. Kim SH, et al. Protective effects of an electrophilic metabolite of docosahexaenoic acid on UVB-induced oxidative cell death, dermatitis, and carcinogenesis. Redox Biol. 2023;62:102666. https://doi.org/10.1016/j.redox.2023.102666.
31. Atwa AM, et al. Candesartan attenuates Cisplatin-Induced Lung Injury by modulating oxidative stress, inflammation, and TLR-4/NF-kappaB, JAK1/STAT3, and Nrf2/HO-1 signaling. Pharmaceuticals (Basel). 2022;15(10). https://doi.org/10.3390/ph15101222.
32. Lee YJ et al. Oxidative stress-induced apoptosis is mediated by ERK1/2 phosphorylation, Exp Cell Res 291(1) (2003) 251 – 66. https://doi.org/10.1016/s0014-4827(03)00391-4
33. Lahair MM, et al. Molecular pathways leading to oxidative stress-induced phosphorylation of Akt. Antioxid Redox Signal. 2006;8(9–10):1749–56. https://doi.org/10.1089/ars.2006.8.1749.
34. Thatikonda S, et al. Piperlongumine regulates epigenetic modulation and alleviates psoriasis-like skin inflammation via inhibition of hyperproliferation and inflammation. Cell Death Dis. 2020;11(1):21. https://doi.org/10.1038/s41419-019-2212-y.
35. Fan G, et al. Gondoic acid alleviates LPS–induced Kupffer cells inflammation by inhibiting ROS production and PKCtheta/ERK/STAT3 signaling pathway. Int Immunopharmacol. 2022;111:109171. https://doi.org/10.1016/j.intimp.2022.109171.
36. Zhao X, et al. A novel adhesive dual-sensitive hydrogel for sustained release of exosomes derived from M2 macrophages promotes repair of bone defects. Mater Today Bio. 2023;23:100840. https://doi.org/10.1016/j.mtbio.2023.100840.
37. Yang Y, et al. Tissue-integratable and biocompatible photogelation by the Imine Crosslinking reaction. Adv Mater. 2016;28(14):2724–30. https://doi.org/10.1002/adma.201505336.
38. Collaborators GBDD. Global, regional, and national burden of diabetes from 1990 to 2021, with projections of prevalence to 2050: a systematic analysis for the global burden of Disease Study 2021. Lancet. 2023;402(10397):203–34. https://doi.org/10.1016/S0140-6736(23)01301-6.
39. Ly HT, et al. Pharmacological properties of Ensete glaucum seed extract: novel insights for antidiabetic effects via modulation of oxidative stress, inflammation, apoptosis and MAPK signaling pathways. J Ethnopharmacol. 2024;320:117427. https://doi.org/10.1016/j.jep.2023.117427.
40. Patel S, et al. Mechanistic insight into diabetic wounds: Pathogenesis, molecular targets and treatment strategies to pace wound healing. Biomed Pharmacother. 2019;112:108615. https://doi.org/10.1016/j.biopha.2019.108615.
41. Schafer M. S Werner 2008 Oxidative stress in normal and impaired wound repair. Pharmacol Res 58 2 165–71 https://doi.org/10.1016/j.phrs.2008.06.004.
42. Forman HJ, et al. Signaling functions of reactive oxygen species. Biochemistry. 2010;49(5):835–42. https://doi.org/10.1021/bi9020378.
43. Tie S, et al. pH-Responsive core-Shell microparticles prepared by a microfluidic chip for the Encapsulation and Controlled Release of Procyanidins. J Agric Food Chem. 2021;69(5):1466–77. https://doi.org/10.1021/acs.jafc.0c04895.
44. Jiang T, et al. Nanobiotechnology: applications in Chronic Wound Healing. Int J Nanomed. 2022;17:3125–45. https://doi.org/10.2147/IJN.S372211.

Publisher's note